Raman Scattering in KNO₃ Phases I, II, and III

M. BALKANSKI, M. K. TENG, AND M. NUSIMOVICI

*Laboratoire de Physique des Solides Equipe de Recherche associée au Centre National de la Recherche
Scientifique Faculté des Sciences de Paris, Paris, France*

The Raman scattering for a complete phase-transition cycle (II → I → III → II) in KNO₃ is reported for the first time, with the intention to correlate the Raman-active modes in different crystalline structures. In addition to the data reported in earlier works, experimental results are obtained for the ferroelectric phase in which we noted a significant increase of intensity for all the covalent modes. A broad band with its half-width depending closely upon the temperature is also observed at 120 cm⁻¹ in this phase. In addition, two new lines at 65 and 133 cm⁻¹ are found in the room-temperature phase. Furthermore, the variation of intensity with various temperatures allows us to follow the scattering of all the observed Raman modes through the different phase transitions during a complete cycle. Using group theory, a study is made to connect various optical modes in the simple ferroelectric phase with corresponding modes in the other two phases. The Raman data presented here, together with previous infrared results, enable us to verify this deduction satisfactorily, at least for the covalent modes.

I. INTRODUCTION

UNDER atmospheric pressure, potassium nitrate exists in three phases depending upon the temperature.[1] The room-temperature phase, or phase II, has the aragonite structure whose space group is D_{2h}^{16}. Above 130°C, the high-temperature phase, or phase I, is generally believed to have the calcite structure whose space group is D_{3d}^6, but no conclusive determination of its structure has been reported to support this argument. When the crystal is cooled, the inverse transition phase I → phase II does not occur directly, but the crystal changes first to another phase at a temperature of 125°C and as the temperature is lowered to 110°C, the crystal transforms again into the room-temperature phase. The intermediate phase, commonly called phase III, has the space group C_{3v}^5 and appears only when the crystal is preliminarily heated to about 180°C. Phase III shows interesting ferroelectric properties and the transition temperatures mentioned above depend upon the history of the sample and the cooling process. In order to study the lattice dynamics of the different phases and their correlations, we believe that the Raman scattering would yield interesting informations about the normal modes of each phase and some of the phase-transition problems.

Recently, the infrared spectra of KNO₃ were investigated by several authors,[2–4]; the data reported by them concern only the high-frequency region. Several Raman-scattering results performed with a mercury source have also been reported in phases II and I.[5–8] Among these,

Nedungadi[5] reported for the aragonite structure the following Raman modes frequencies: 52, 82, 100, 126, 143, 714, 1050, 1343, and 1361 cm⁻¹. The first five low-frequency lines correspond to the relative vibrations of the ions and the remaining four lines were attributed to the internal vibrations of the NO₃⁻ ion. Furthermore, he observed that some of the low-frequency modes broadened out and practically all disappeared at 120°C. These measurements in the high-temperature range were performed with unpolarized light. Chisler[8] observed the appearance of an opalescence in the temperature range 130–180°C, which was not mentioned by Nedungali in his work.

In a previous paper,[9] we gave a general study of the symmetry properties of the three phases of KNO₃ and also studied the selection rules for the interactions between the lattice vibrations and the radiation field—infrared absorption and Raman scattering.

In the present paper, we report Raman-scattering data of KNO₃ in its three phases obtained using a He-Ne laser source. For the first time, Raman data of a complete phase-transition cycle are reported, particularly those of the ferroelectric phase. Furthermore, two new lines at 65 and 133 cm⁻¹ are found in addition to those reported by Nedungadi in the room-temperature phase.

Starting from the idea that there exists a relation between normal modes of different phases when crystal goes from one structure to another, we try to connect modes in the simple ferroelectric phase with the corresponding modes in the other two phases by following the Raman scattering of various modes of vibration.

II. THEORETICAL BACKGROUND

A. Classification of the Optical Modes

Let us consider an ionic crystal composed of nitrate and potassium ions. The optical modes of vibration of this crystal can be classified into three categories.

[1] See, e.g., S. Sawada, S. Nomura, and Y. Asao, J. Phys. Soc. Japan **16**, 2486 (1961).
[2] S. V. Karpov and A. A. Shultin, J. Phys. Chem. Solids **29**, 475 (1968).
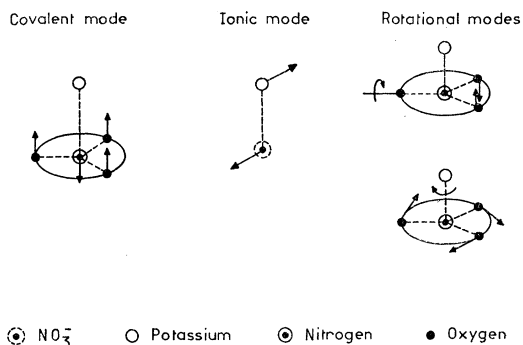[3] A. Grynwald (private communication).
[4] T. Yanagi, J. Phys. Soc. Japan **20**, 1351 (1965).
[5] T. M. K. Nedungadi, Proc. Indian Acad. Sci. **A14**, 242 (1942).
[6] L. Couture, Compt. Rend. Acad. Sci. Paris **656**, (1945).
[7] E. V. Chisler, Fiz. Tverd. Tela **7**, 1586 (1965) [English transl.: Soviet Phys.—Solid State **7**, 1283 (1965)].
[8] E. V. Chisler, Fiz. Tverd. Tela **8**, 1938 (1966) [English transl.: Soviet Phys.—Solid State **8**, 1534 (1966)].

[9] M. Nusimovici, in *Proceedings of the International Meeting on Ferroelectricity, 1966* (Elsevier Publishing Company, Inc., Amsterdam, 1967).

Covalent mode   Ionic mode   Rotational modes

⊙ NO$_3^-$ O Potassium   ◉ Nitrogen   ● Oxygen

FIG. 1. The three categories of normal modes of vibration in KNO$_3$.

(i) The ionic modes, in which the nitrate and the potassium are considered as rigid point ions, and the modes of vibration are those of a pure ionic crystal.

(ii) The covalent modes associated with the molecular vibrations of the nitrate ion regarded as a molecule in which the atoms are bound by covalent forces.

(iii) The rotational modes, in which the nitrate ion is considered as a rigid rotator. These normal modes are due to the rotation of the nitrate ion around its c.m. Those modes are neither ionic modes since there is no relative motion of the c.m. of the anion and the cation, nor covalent modes since there is no deformation of the nitrate ion. They correspond to a very low energy.

It must be mentioned that Bhagavantam[10] has classi-fied the modes of vibration in two categories. (i) The lattice modes or external modes of low energy corre-spond to ionic and rotational modes; and (ii) the inter-nal modes of high energy correspond to the covalent modes.

An example of the three categories of modes con-sidered here is illustrated on Fig. 1.

B. Group Properties and Selection Rules

Assuming that the potassium nitrate has the calcite structure in phase I, then the space groups correspond-ing to phases I, II, and III are, respectively, D_{3h}^6, D_{2h}^{16}, and C_{3v}^5. We give in Table I the character tables of the factor groups of potassium nitrate.

The representation of the ionic modes Γ_i is that of a linear vector space based on the optical vibrations of the nitrate and potassium ions considered as rigid.

In phase I, the unit cell contains four ions; therefore, the dimension of Γ_i is $4 \times 3 - 3 = 9$. In phase II, the unit cell contains eight ions; therefore, the dimension of Γ_i is $8 \times 3 - 3 = 21$. In phase III, the unit cell con-tains two ions; therefore, the dimension of Γ_i is $2 \times 3 - 3 = 3$. In the following equations, we give the reduction of Γ_i in terms of irreducible representations of the crystal group.

[10] S. Bhagavantam, Proc. Indian Acad. Sci. **13**, 543 (1941).

TABLE I. Character tables of the representations of the factor groups of C_{3v}^5, D_{3d}^6, and D_{2h}^{16}.

C_{3v}^5	E	$2C_3$	$3\sigma_v$
Γ_1	1	1	1
Γ_2	1	1	−1
Γ_3	2	−1	0

D_{3d}^6	E	$2C_3$	$3\sigma_v$	I	$2S_6$	$3C_2$
Γ_1	1	1	1	1	1	1
Γ_2	1	1	−1	1	1	−1
Γ_3	2	−1	0	2	−1	0
Γ_4	1	1	1	−1	−1	−1
Γ_5	1	1	−1	−1	−1	1
Γ_6	2	−1	0	−2	1	0

D_{2h}^{16}	E	C_z	C_y	C_x	I	σ_z	σ_y	σ_x
Γ_1	1	1	1	1	1	1	1	1
Γ_2	1	1	1	1	−1	−1	−1	−1
Γ_3	1	−1	1	−1	1	−1	1	−1
Γ_4	1	−1	1	−1	−1	1	−1	1
Γ_5	1	1	−1	−1	1	1	−1	−1
Γ_6	1	1	−1	−1	−1	−1	1	1
Γ_7	1	−1	−1	1	1	−1	−1	1
Γ_8	1	−1	−1	1	−1	1	1	−1

Phase I[11]

$$\Gamma_i = \Gamma_2 + {}^2\Gamma_3 + \Gamma_4 + \Gamma_5 + {}^2\Gamma_6;$$

Phase II

$$\Gamma_i = 4\Gamma_1 + 2\Gamma_2 + 4\Gamma_3 + \Gamma_4 + 2\Gamma_5 + 3\Gamma_6 + 2\Gamma_7 + 3\Gamma_8;$$

Phase III

$$\Gamma_i = \Gamma_1 + {}^2\Gamma_3.$$

The representation of the covalent and rotational modes is that of a linear vector space based on the vibrations of oxygen atoms in the nitrate ion. In this vector space, the rotation associated with each nitrate ion is three-dimensional. Therefore, the representation of the rotational modes Γ_r is $3m$-dimensional, where m represents the number of nitrate ions per unit cell. The dimension of the representation of the covalent modes Γ_c is then equal to $3(n-m)$, where n refers to the number of oxygen atoms in the unit cell.

In phase I, there are two nitrates per cell; therefore, the dimension of Γ_r is 6 and that of Γ_c is 12. In phase II, there are four nitrates per cell; therefore, the dimension of Γ_r is 12 and that of Γ_c is 24. In phase III, there is only one nitrate per cell; therefore, the dimension of Γ_r is 3 and that of Γ_c is 6.

The following equations give the reduction of Γ_r and Γ_c:

Phase I

$$\Gamma_r = \Gamma_2 + {}^2\Gamma_3 + \Gamma_4 + {}^2\Gamma_6,$$
$$\Gamma_c = \Gamma_1 + \Gamma_2 + 2{}^2\Gamma_3 + \Gamma_4 + \Gamma_5 + {}^2\Gamma_6;$$

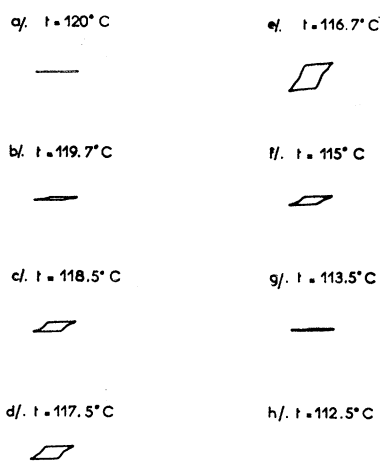[11] The superscript 2 indicates that the mode is doubly degenerate.

FIG. 2. D-E hysteresis loops (E horizontal, D vertical) of KNO_3 measured along the c axis when the crystal is cooled ($E_{max}=3.7$ kV/cm).

Phase II

$$\Gamma_r = \Gamma_1 + 2\Gamma_2 + \Gamma_3 + 2\Gamma_4 + 2\Gamma_5 + \Gamma_6 + 2\Gamma_7 + \Gamma_8,$$

$$\Gamma_c = 4\Gamma_1 + 2\Gamma_2 + 4\Gamma_3 + 2\Gamma_4 + 2\Gamma_5 + 4\Gamma_6 + 2\Gamma_7 + 4\Gamma_8;$$

Phase III

$$\Gamma_r = \Gamma_2 + {}^2\Gamma_3,$$

$$\Gamma_c = 2\Gamma_1 + 2^2\Gamma_3.$$

The selection rules for all these vibrational modes with regard to a Raman process are determined by the representation of the polarizability tensor α. In Table II, we give the representation of the nonvanishing components of α in the three phases of KNO_3. In an experiment where the incident light is polarized in the ith direction and the scattered light in the jth direction, the polarizability tensor component involved is then α_{ij} and those modes are active which correspond to irreducible representations of α_{ij} given in Table II.

Axes x, y, and z are defined as follows: The z axis is normal to the plane of the nitrate. In phases I and III, the x and y axes can be any axis normal to the c axis of the crystal. In phase II, which is biaxial, the unit cell is a parallelepiped of dimensions $a=5.43$, $b=9.17$, and $c=6.45$ Å. The x axis has been chosen parallel to side b, the y axis parallel to side a, and the z axis, normal to the plane of nitrate, is parallel to c.

III. EXPERIMENTAL PROCEDURE

The experimental apparatus consists of a 50-mW-He-Ne gas laser source ($\lambda = 6328$ Å), a double-grating monochromator CODERG, and a system of focusing lens and mirrors allowing the collection of at least three passages of the incident beam through the crystal. The scattered light is collected at right angles from the incident direction and is focused into the spectrometer entrance slit and detected by an S20 photomultiplier. The signal of the photomultiplier is finally amplified

TABLE II. Representations of the nonvanishing components of the polarizability tensor of KNO_3 in phases I, II, and III.

	Phase I	Phase II	Phase III
α_{xx}	$\Gamma_1 \oplus \Gamma_3$	Γ_1	$\Gamma_1 \oplus \Gamma_3$
α_{yy}	$\Gamma_1 \oplus \Gamma_3$	Γ_1	$\Gamma_1 \oplus \Gamma_3$
α_{zz}	Γ_1	Γ_1	Γ_1
α_{xy}	Γ_3	Γ_5	Γ_3
α_{xz}	Γ_3	Γ_3	Γ_3
α_{yz}	Γ_3	Γ_7	Γ_3

and recorded. Measurements are performed with both incident and scattered lights polarized. The slit width used in our investigation corresponds to a spectral separation of about 3, 6, or 20 cm^{-1} according to the intensity of the observed lines.

The temperature of the sample whose dimension is about $7 \times 5 \times 5$ mm is controlled during both heating and cooling. The sample is sandwiched between two metal plates heated by an electric resistor. The experimental error of the temperature of the heating plates is estimated to about 0.5°C and the temperature of the sample is thus determined with an error of about 1°C.

In order to determine the actual temperature range corresponding to the ferroelectric phase III in our crystal, we measured the D-E hysteresis loops at various temperatures on cooling. Figure 2 shows the results obtained in this experiment. The crystal is first heated gradually from room temperature to 115°C, then slowly at the rate of 1°C/h from 115 to 140°C, and finally with a faster speed from 140 to 180°C. The cooling process is quite similar to the heating process: The crystal is cooled gradually from 180 to 132°C, then very slowly between 132 to 100°C, and finally with a faster speed down to room temperature.

The notation $Y(ZY)X$ used here is the one adopted by Porto et al.[12] In this notation, the wave vector of the incident light is parallel to the y axis, the wave vector of the scattered light is parallel to the x axis, the incident light is polarized along the z axis, and the scattered light is polarized along the y axis. The polarizability tensor component involved is then α_{zy}.

IV. EXPERIMENTAL RESULTS

Results are first reported for phase II, stable at room temperature; then for phase I, obtained by heating the crystal; and finally for the ferroelectric phase III, obtained by cooling.

A. Phase II

Selection rules show that there are 30 Raman-active modes in this phase; 12 of them are actually observed. Figure 3 shows the most intense Raman lines of KNO_3 in this aragonite structure. The corresponding frequencies are 50, 83, and 1054 cm^{-1}.

[12] S. P. S. Porto, J. A. Giordamaine, and T. C. Damen, Phys. Rev. 147, 608 (1966).

Since no line is found between 200 and 700 cm⁻¹, only spectra in the spectral range extending to about 200 cm⁻¹ from the laser frequency are shown (Fig. 4). From these spectra five Raman lines are found at the frequencies 65, 103, 122, 133, and 138 cm⁻¹. The two lines 65 and 133, which have not been reported in earlier works, were also verified by observing their anti-Stoke component.

Figure 5(a) shows the polarizations in which the line at 714 cm⁻¹ is excited, and Fig. 5(b) represents the last two lines occuring at 1348 and 1362 cm⁻¹.

Several crystal orientations have been used in our investigation. The relative intensity of the observed Raman lines are given in Table III in which the intensity of the strongest of them has been arbitrary—chosen equal to 1000.

For the covalent modes occuring at high frequencies, the examination of the Table III shows that the line at 714 cm⁻¹ has a doublet structure consisting of two covalent modes (Γ_1 and Γ_5). The set of two lines at about 1350 cm⁻¹ has been well separated: The 1348 line corresponds to a Γ_5 mode and the 1362 line to a Γ_1 mode. Finally, the totally symmetric line at 1054 cm⁻¹ has been unambiguously assigned to a Γ_1 mode with $\alpha_{zz} \ll \alpha_{xx} \simeq \alpha_{yy}$. This relation is consistent with all the other observed Γ_1 modes.

The lines at 50, 65, and 83 cm⁻¹ occurring at relatively low frequencies might be due to rotational modes. As has been suggested,[5,6] the lines 50 and 83 which are strongly excited in (ZY) and (ZX) polarizations, respectively, might be attributed to two rotational modes Γ_7 and Γ_3 corresponding to rotation of the nitrate planes about the x and y axes. The line at 65 cm⁻¹, which is excited in (XY) polarization, may be due to a
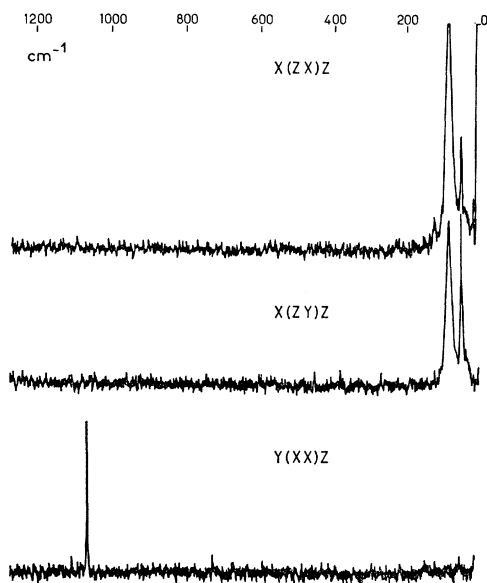

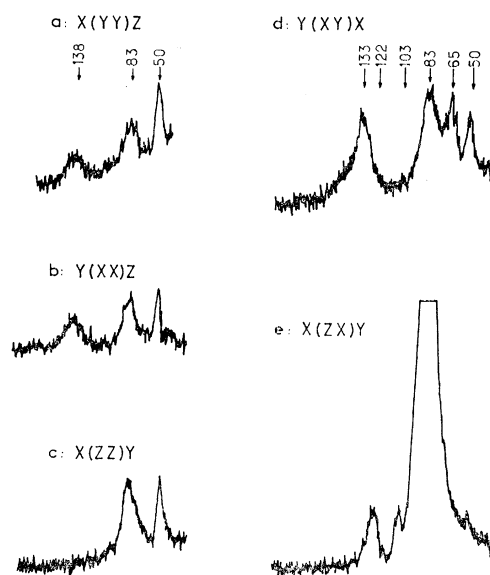FIG. 4. Raman spectra of aragonite KNO₃ from 0 to 200 cm⁻¹: (a), (b), (c), and (d), are performed with 6 cm⁻¹ slit width; (e) is performed with 3 cm⁻¹ slit width.

Γ_5 rotational mode related to rotation of the nitrate planes about the z axis.

Furthermore, we observed one Γ_1 mode at 138 cm⁻¹, two Γ_3 modes at 103 and 122 cm⁻¹, and one Γ_5 mode at 133 cm⁻¹. The frequency range in which these modes are observed and their low intensity suggest that they are related to ionic modes.

It must be mentioned that there are an important α_{zx} component of line 50 and an important α_{zy} com-

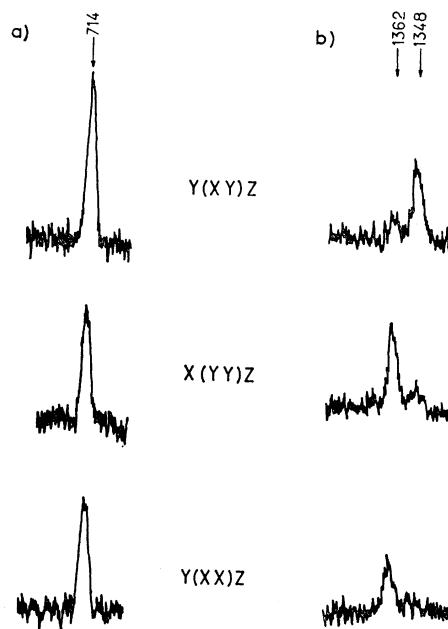FIG. 3. Raman spectra of aragonite KNO₃ (phase II) performed with 3 cm⁻¹ slit width.

FIG. 5. Raman spectra of aragonite KNO₃ showing the lines 714, 1348, and 1362 cm⁻¹, and performed with 6 cm⁻¹ slit width.

TABLE III. Observed intensities of the components of the polarizability tensor in argonite KNO_3 (phase II).

Polarization \ Frequency in cm⁻¹	50	65	83	103	122	133	138	714	1054	1348	1362
$X(YY)Z$	60	0	50	0	0	0	50	70	650	0	60
$X(ZX)Z$	300	0	1000	70	100	0	0	0	0	0	0
$X(ZY)Z$	650	0	700	0	0	0	0	0	0	0	0
$X(YX)Z$	60	80	80	0	0	60	0	100	250	50	0
$Y(XX)Z$	50	0	70	0	0	0	70	70	650	0	40
$Y(ZX)Z$	250	0	750	50	100	0	0	0	0	0	0
$Y(ZY)Z$	750	0	750	0	0	0	0	0	0	0	0
$Y(XY)Z$	50	50	50	0	0	50	0	100	250	50	0
$Y(ZZ)X$	70	0	70	0	0	0	0	0	100	0	0
$Y(XZ)X$	40	0	1000	70	120	0	0	0	20	0	0
$Y(XY)X$	40	80	80	0	0	100	0	120	20	50	0
$X(ZZ)Y$	70	0	80	0	0	0	0	0	120	0	0
$X(ZX)Y$	50	0	1000	150	200	0	0	0	20	0	0

ponent of line 83 for crystal orientations in which the nitrate plane does not coincide with the scattering plane. A non-negligible α_{xy} component is also observed for the totally symmetric Γ_1 at 1054 cm⁻¹. As has been suggested by Porto et al. in the case of calcite,[12] this anomaly may be motived by the high beam convergence. By supressing all the focusing lens in the passage of the laser beam, we noticed also a notable decrease of the apparent depolarization of these lines. On the other hand, a misorientation of the crystal is always possible. Then, we believe that the above anomaly would be caused by all these unavoidable experimental errors.

B. Phase I

If the calcite structure (D_{3d}^6) is the suitable one for this phase, nine Raman-active modes will be foreseen,

five of them experimentally observed. The crystal was oriented with OY directed along the incident direction and OX along the scattered direction. Furthermore, in order to follow the observed modes from one phase to another, and on account of the large number of spectra performed to study phases I and III, only some of them have been shown and we present the data by means of intensity diagrams plotted versus various temperatures.

Figure 6 shows that for the covalent modes, while the lines at 714 and 1056 cm⁻¹ remain easily observable in spite of a notable decrease of intensity, the line at 1348 cm⁻¹ disappears completely above 130°C and a new line occuring at 1428 cm⁻¹ is observed. The measurements of the polarizability tensor components indicate that lines 714 and 1428 are related to two doubly degenerate Γ_3 modes and line 1056 is associated with a Γ_1 mode.
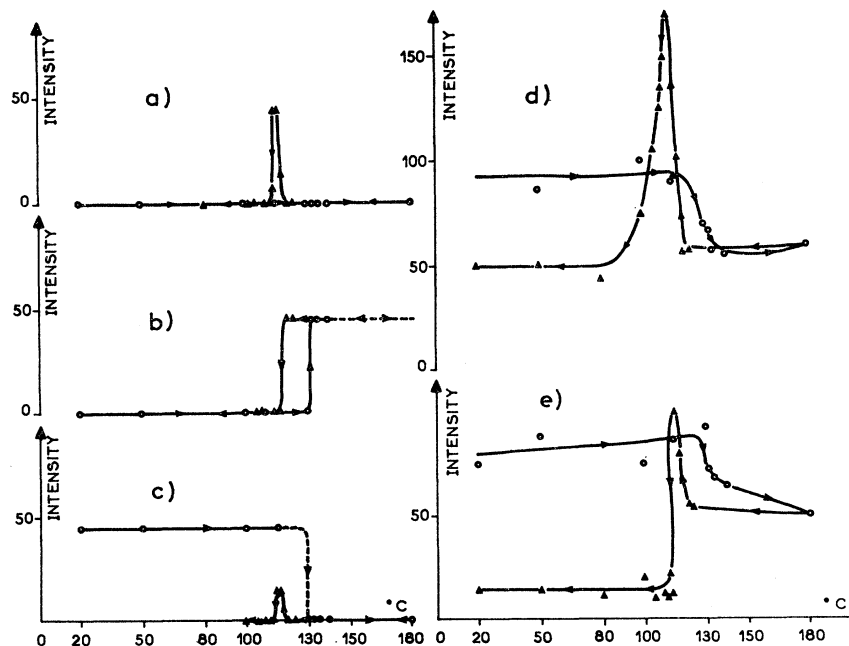

FIG. 6. Intensity diagram of the covalent modes of KNO_3 as a function of the temperature. The open circles represent data when the crystal is heated, and the triangles when the crystal is cooled. The arrows indicate the sense of increasing or decreasing temperature: (a) line at 1434 cm⁻¹, (b) line at 1428 cm⁻¹, (c) line at 1348 cm⁻¹, (d) line at 1057 cm⁻¹, and (e) line at 714 cm⁻¹.

FIG. 7. Intensity diagram of the ionic and rotational modes of KNO$_3$ with various temperatures: (a) line at 120 cm^{-1}, (b) line at 83 cm^{-1} performed with $Y(ZY)X$ polarization, (c) line at 83 cm^{-1} performed with $Y(XZ)Y$ polarization, and (d) line at 50 cm^{-1}.
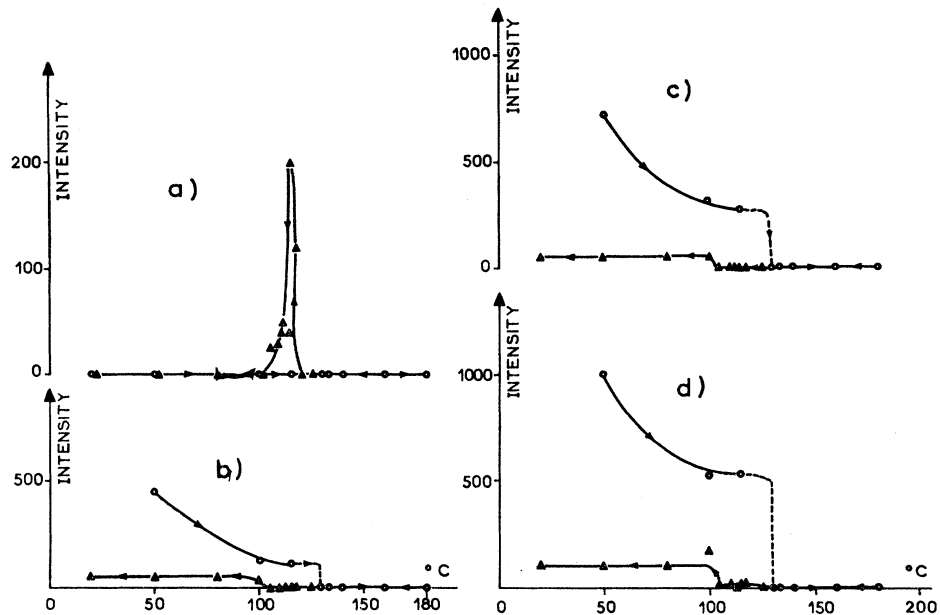
All the ionic and rotational modes observed in phase II disappear abruptly when the temperature approaches the II → I transition point; we do not observe any new line in the low-frequency region (Fig. 7).
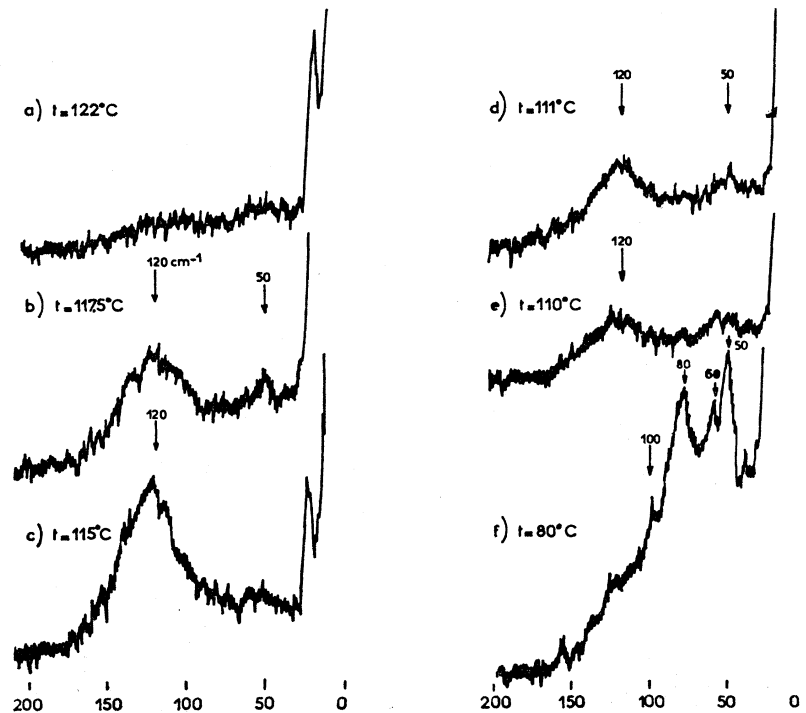
C. Phase III

For the ferroelectric phase $(C_{3v}{}^5)$, selection rules predict 11 modes that are active both in Raman scattering and infrared absorption, seven of them observed experimentally.

In the high-frequency region, we observed two doubly degenerate Γ_3 modes at 716 and 1352 cm^{-1} and one Γ_1 mode at 1057 cm^{-1} (Fig. 6). In addition, one notes the presence of a line occuring at 1434 cm^{-1} which is active in all the four polarizations used in this experiment $(\alpha_{zz}, \alpha_{zy}, \alpha_{zx},$ and $\alpha_{xy})$ and corresponds to a mixed Γ_1 and Γ_3 symmetry character.

In the low-frequency range, the most striking feature is the observation of a broad band with intensity maximum at 120 cm^{-1} and a Γ_3 symmetry character. While

FIG. 8. Spectra showing the temperature dependence of the line at 120 cm^{-1} in phase III when cooling and performed with a 6-cm^{-1} slit width.
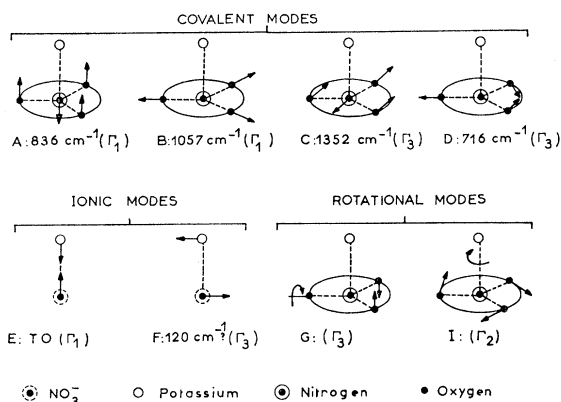
FIG. 9. Scheme of the optical modes of vibration in ferroelectric KNO_3 (phase III).

FIG. 10. Scheme of the totally symmetric mode B in ferroelectric phase and its corresponding modes in phases I and II.

the half-width of this band changes closely with temperature, its frequency, however, remains constant in the temperature range covering phase III (Fig. 8).

It must be mentioned that in this ferroelectric phase, the intensity of all the covalent modes exhibits a notable increase, reaching a maximum at about 115°C, except for the 1057 line for which the maximum occurs only at about 112°C (Fig. 6).

V. INTERPRETATION

In order to establish the correlation between vibrational modes in the three phases under consideration, we start from the simplest of them, phase III. We will ultimately orient the study of the determination of normal modes and their interpretation in the two other phases by basing our treatment on the modes already determined in phase III. Accordingly, a more detailed interpretation will be devoted to this ferroelectric phase.

A. Phase III

In Fig. 9 we give the scheme of vibration of the various optical modes in phase III with their symmetry. Just as the classification of the optical modes into three categories in Sec. I, the scheme of vibrations in Fig. 9 is intended to facilitate our study in following the modes from one phase to another. Some of the true normal modes may be a normalized linear combination of all the modes of same symmetry.

Since the symmetry of an isolated nitrate ion corresponds to D_{3h} point group and the interacting forces are much stronger in the nitrate ion than between the nitrate and potassium ions, the identification of the covalent modes A, B, C, and D, is easy. They are closely related to the well-known ν_2, ν_1, ν_3, and ν_4 modes of the D_{3h} point group[13] with $\omega_A = 836$ cm^{-1}(Γ_1),[14] $\omega_B = 1054$ cm^{-1} (Γ_1), $\omega_C = 1352$ cm^{-1} (Γ_3), and $\omega_D = 716$ cm^{-1} (Γ_3).

The mode at 1434 cm^{-1} satisfies selection rules for both Γ_1 and Γ_3; therefore, this frequency cannot be attributed to a one-phonon process of well-defined symmetry. As was pointed out by Loudon,[15] the frequency shift that occurs in a two-phonon line spectrum is the sum and difference of the shifts that occur in the first-order spectrum and the wave vectors of the involved phonons in such a process must be small. It is possible to assign this band to a two-phonon process involving an overtone of the mode D: $2\omega_D = 1432$ cm^{-1}. Moreover, we have $\Gamma_3 \times \Gamma_3 = \Gamma_1 + \Gamma_2 + \Gamma_3$; therefore, $2\omega_D$ is active in both Γ_1 and Γ_3 symmetries.

At 120 cm^{-1} we observe a broad band having a half-width of about 40 cm^{-1} and a Γ_3 symmetry character. Two degenerate Γ_3 modes are Raman active in the low-frequency region, the ionic mode F and the rotational mode G. The relatively strong intensity of the observed band and the very close variation of its half-width with temperature seem to encourage the assignment of the rotational mode G. From an other point of view, mode G, which corresponds to the vibration of the nitrate plane around an axis perpendicular to the z direction, would occur at lower frequency in phase II (about 80 cm^{-1}); now it happens that no shifting toward a low-frequency region of the observed band has been noted, even in the temperature range covering the III $\rightarrow$ II phase transition: The frequency of the band remains always constant and equal to 120 cm^{-1}. Moreover, some partial infrared data indicate that an ionic mode is observed near 120 cm^{-1} in the high-temperature range.[3] Therefore, the assignment of the ionic mode F seems favored by these last arguments. Just as for the mode E that will be discussed in the next paragraph, further infrared results in the low-frequency range will be useful to settle definitively this question.

[13] G. Herzberg, *Molecular Spectra and Molecular Structure* (D. Van Nostrand Inc., New York, 1945), Vol. 2.

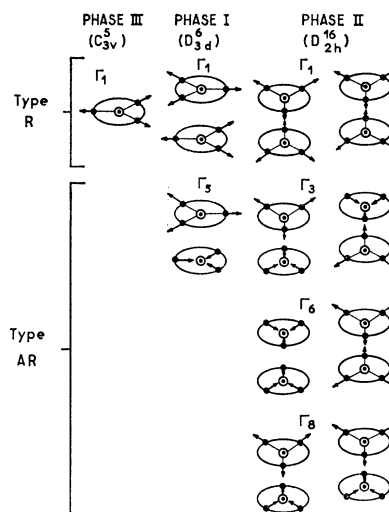[14] This mode has been found in an infrared experiment (Ref. 2).

[15] R. Loudon, Advan. Phys. **13**, 423 (1964).

TABLE IV. Correlation between the optical modes in phase III and their corresponding modes of type R in phases I and II. Comparison with experimental results.

		Phase I		Phase II		Phase III	
		Corresponding modes predicted by group theory	Observed frequency in cm⁻¹	Corresponding modes predicted by group theory	Observed frequency in cm⁻¹	Corresponding modes predicted by group theory	Observed frequency in cm⁻¹
	A	$\Gamma_4(I)$ᵃ	836⁺(Γ_4)ᵇ	$\Gamma_6(I)$ᵃ	829⁺(Γ_6)ᵇ	$\Gamma_1(R,I)$ᶜ,ᵃ	836⁺(Γ_1)ᵇ
Covalent	B	$\Gamma_1(R)$ᶜ	1056(Γ_1)	$\Gamma_1(R)$ᶜ	1054(Γ_1)	$\Gamma_1(R,I)$ᶜ,ᵃ	1057(Γ_1), 1053⁺(Γ_1)ᵇ
modes	C	$\Gamma_3(R)$ᶜ	1428(Γ_3)	$\Gamma_1(R)$,ᶜ $\Gamma_5(R)$ᶜ	1362(Γ_1), 1348(Γ_5)	$\Gamma_3(R,I)$ᶜ,ᵃ	1352(Γ_3)
	D	$\Gamma_3(R)$ᶜ	714(Γ_3)	$\Gamma_1(R)$ᶜ, $\Gamma_5(R)$ᶜ	714(Γ_1 and Γ_5)	$\Gamma_3(R,I)$ᶜ,ᵃ	716(Γ_3), 717⁺(Γ_3)ᵇ
Ionic	E	$\Gamma_4(I)$ᵃ		$\Gamma_1(R)$ᶜ	138(Γ_1)	$\Gamma_1(R,I)$ᶜ,ᵃ	
modes	F	$\Gamma_6(I)$ᵃ		$\Gamma_4(I)$,ᵃ $\Gamma_8(I)$ᵃ		$\Gamma_3(R,I)$ᶜ,ᵃ	120(Γ_3)?
Rotational	G	$\Gamma_3(R)$ᶜ		$\Gamma_3(R)$,ᶜ $\Gamma_7(R)$ᶜ	83(Γ_3), 50(Γ_7)	$\Gamma_3(R,I)$ᶜ,ᵃ	120(Γ_3)?
modes	I	$\Gamma_2(f)$ᵈ		$\Gamma_5(R)$ᶜ	65(Γ_5)	$\Gamma_2(f)$ᵈ	

ᵃ I: Allowed in infrared absorption.
ᵇ +: Observed in infrared experiment (Ref. 2).
ᶜ R: Allowed in Raman scattering.
ᵈ f: Forbidden in both Raman scattering and infrared absorption.

No ionic mode was found in the Γ_1 symmetry. This fact may be due to the ferroelectricity of phase III; mode E, having Γ_1 symmetry, is a TO mode, the frequency of which should be very small at the center of the Brillouin zone for a ferroelectric crystal. However, it is difficult at present to make such an assumption because of the fact that the corresponding mode is not Raman active in the paraelectric phase I. Therefore its frequency shift cannot be followed through the I → III phase transition. Further investigations, in which this mode would be rendered Raman active and its frequency shifted in the temperature range covering the paraferroelectric phase transition, would yield valuable information concerning this mode.

B. Phases I and II

Starting from the modes A, B, C, D, E, F, G, and I, in phase III, we try to deduce the representations of normal modes in the two other phases that correspond to each of the above modes. Let us consider that the crystal passes from phase III to phase II via phase I, the number of molecules per unit cell passes from one to four, and its structure changes from lower to higher symmetry. Then, a given mode in phase III can give rise to several modes in phases I and II. Among them, one can distinguish two types of modes: For the first one, each molecule of the unit cell vibrates in the same manner as the mode from which it is derived and all the molecules in the unit cell vibrate in phase to each other; for the second one, although the individual molecule in the unit cell vibrates in the same manner as the original mode, the different molecules in the unit cell move in opposite phases to each other. We will call the first type of modes R type and the second AR type. An example of these two types of modes is illustrated in Fig. 10 for mode B.

Based on the idea that the modes of type AR would give rise to relatively weak intensity even though they are allowed by selection rules, we try to interpret the results in phases I and II by using this assumption.

The results deduced by group theory for optical modes of type R are listed in Table IV and those of type AR are listed in Table V.

Inspection of Table IV shows that for covalent modes all the predicted Raman-active modes of type R are observed, and that the correspondence between all these modes is firmly evidenced. For the ionic modes of type R the assignment of mode Γ_1 at 138 cm⁻¹ in phase II is also unambiguously proven, since there is only one Γ_1 mode that is Raman active in this phase. For the rotational modes there is nevertheless a discrepancy for mode G: We do not observe the corresponding Γ_3 mode that is allowed by selection rules in phase I. Since in the paraelectric phase an orientational disorder of the nitrate ions exists in the plane perpendicular to the z axis,[16] this mode may be probably altered by this disorder. Furthermore, Table V shows that three ionic modes of type AR are also observed in the room-temperature phase II.

VI. DISCUSSION

In order to develop a more general discussion, some available infrared data are also listed in Tables IV and V for comparison. It is evident from this comparison that there is perfect agreement between theoretical provisions and experimental results concerning the covalent modes of type R. The absence of Raman data for mode A and infrared data for mode C in phase III is due to the fact that they have not been studied by the authors. Besides, some covalent modes of type AR are also observed in infrared experiment with weaker intensity. As expected, the covalent modes, which are essentially related to internal vibrations of the nitrate ion, would produce no significant change when the crystal goes from one phase to another; one can easily follow such modes through different phase transitions as shown in Fig. 6.

[16] Y. Shinnaka, J. Phys. Soc. Japan 17, 820 (1962).

TABLE V. Correlation between the optical modes in phase III and their corresponding modes of type AR in phases I and II. Comparison with experimental results.

		Phase I		Phase II	
		Corresponding modes predicted by group theory	Observed frequency in cm^{-1}	Corresponding modes predicted by group theory	Observed frequency in cm^{-1}
Covalent modes	A	$\Gamma_2(f)$[a]		$\Gamma_1(R)$,[b] $\Gamma_3(R)$,[b] $\Gamma_8(I)$[c]	$846^+(\Gamma_8)$[d]
	B	$\Gamma_5(f)$[a]		$\Gamma_3(R)$,[b] $\Gamma_6(I)$,[c] $\Gamma_8(I)$[c]	$1051^+(\Gamma_6)$,[d] $1049.9^+(\Gamma_8)$[d]
	C	$\Gamma_6(I)$[c]		$\Gamma_2(f)$,[a] $\Gamma_3(R)$,[b] $\Gamma_4(I)$,[c] $\Gamma_6(I)$,[c] $\Gamma_7(R)$,[b] $\Gamma_8(I)$[c]	
	D	$\Gamma_6(I)$[c]	$716^+(\Gamma_6)$[d]	$\Gamma_2(f)$,[a] $\Gamma_3(R)$,[b] $\Gamma_4(I)$,[c] $\Gamma_6(I)$,[c] $\Gamma_7(R)$,[b] $\Gamma_8(I)$[c]	$714.5^+(\Gamma_4)$,[d] $715.2^+(\Gamma_8)$[d]
Ionic modes	E	$\Gamma_2(f)$,[a] $\Gamma_5(f)$[a]		$\Gamma_3(R)$,[b] $\Gamma_6(I)$,[c] $\Gamma_8(I)$[c]	$103(\Gamma_3)$
	F	$\Gamma_3(R)$,[b] $\Gamma_6(I)$[c]		$\Gamma_1(R)$,[b] $\Gamma_2(f)$,[a] $\Gamma_3(R)$,[b] $\Gamma_5(R)$,[b] $\Gamma_6(I)$,[c] $\Gamma_7(R)$[b]	$122(\Gamma_3), 133(\Gamma_5)$
Rotational modes	G	$\Gamma_6(I)$[c]		$\Gamma_1(R)$,[b] $\Gamma_2(f)$,[a] $\Gamma_4(I)$,[c] $\Gamma_5(R)$,[b] $\Gamma_6(I)$,[c] $\Gamma_8(I)$[c]	
	I	$\Gamma_4(I)$[c]		$\Gamma_2(f)$,[a] $\Gamma_4(I)$,[c] $\Gamma_7(R)$[b]	

[a] f: Forbidden in both Raman scattering and infrared absorption.
[b] R: Allowed by Raman scattering.
[c] I: Allowed by infrared absorption.
[d] +: Observed in infrared experiment (Ref. 2).

For the ionic and rotational modes, unfortunately the lack of experimental results, mainly in infrared absorption, does not allow us to pursue the discussion. Further investigations would be helpful to complete this study.

Finally, several remarks concerning the different phase transitions studied in this work must be made.

On heating, all the ionic and rotational modes in phase II vanish abruptly at 130°C, suggesting that the transition II → I is of a rather sudden nature. A notable and continuous broadening of the rotational mode at 83 cm^{-1} is also observed when the temperature approaches the transition point.

In phase I, we do not observe the appearance of opalescence in the temperature range 130–180°C as reported by Chisler.[8] We did observe that a single crystal of smaller size exhibited opalescence in the temperature range 100–120°C upon heating. It is possible that this phenomenon depends closely upon the quality and the dimension of the sample and possibly also upon the manner in which the crystal is heated.

Between 110 and 100°C on cooling, the general aspect of the spectra suggests that in this region the limits between phases III and II may be less precise, and the III → II phase transition probably occurs more gradually than for the other phase transitions.

When cooling from 110°C to room temperature, the spectra show the reappearance of all the ionic and rotational modes that are previously observed in phase II before the phase-transition cycle. The intensity measurements in this temperature range cannot be compared quantitatively with those given by phase II before heating since the crystal begins to exhibit some cracking and fractures at about 90°C; nevertheless, they are sufficiently strong to confirm the existence of these modes.

VII. CONCLUSION

The Raman-scattering spectra were obtained for the three phases of KNO$_3$. Using group-theoretical considerations, an attempt was made to connect the different optical-active modes in the ferroelectric phase to the corresponding normal modes in the two other phases. The experimental data of all the three phases were then interpreted in a quite satisfactory manner from this assumption.